A Posteriori Analysis of an IMEX Entropy-Viscosity Formulation for Hyperbolic Conservation Laws with Dissipation

Jehanzeb H. Chaudhry[1], John N. Shadid[1,b], Timothy Wildey[c]

[a] *Department of Mathematics and Statistics, The University of New Mexico, Albuquerque, NM 87131*

[b] *Computational Mathematics Department, Sandia National Laboratories, Albuquerque, NM 87123*

[c] *Optimization and Uncertainty Quantification Department, Center for Computing Research, Sandia National Laboratories, Albuquerque, NM 87185. Sandia National Laboratories is a multimission laboratory managed and operated by National Technology and Engineering Solutions of Sandia, LLC., a wholly owned subsidiary of Honeywell International, Inc., for the U.S. Department of Energy's National Nuclear Security Administration under contract DE-NA-0003525. The views expressed in the article do not necessarily represent the views of the U.S. Department of Energy or the United States Government.*

Abstract

This study considers adjoint based a posteriori estimation of the error in a quantity of interest computed from numerical solutions based on multistage implicit-explicit (IMEX) time integration schemes and an entropy-viscosity formulation for damped hyperbolic partial differential equations (PDEs). Hyperbolic systems are challenging to solve numerically due to the need to stabilize systems with discontinuous or nearly discontinuous solutions in an attempt to limit non-physical oscillations and provide accurate solutions. The goal of this effort is to provide error estimates based on adjoint operators, variational analysis and computable residuals. The error estimates quantify the total error as well as different contributions to the error arising from the time integration schemes and choices of numerical parameters in the numerical method.

Keywords: *A posteriori* error estimation, adjoint operator, hyperbolic partial differential equations, finite element method, entropy-viscosity

1. Introduction

This paper is concerned with accurate a posteriori error estimation of numerical solutions of a scalar hyperbolic PDE with dissipation obtained using IMEX

Email addresses: jehanzeb@unm.edu (Jehanzeb H. Chaudhry), jnshadi@sandia.gov (John N. Shadid), tmwilde@sandia.gov (Timothy Wildey)

time integration and an entropy-viscosity method. In particular, we consider a first order hyperbolic scalar conservation law with a small damping/dissipation term

$$\begin{cases} u_t(x,t) + \nabla \cdot f(u(x,t)) = \epsilon \nabla^2 u(x,t), \quad t \in (0,T], x \in \Omega \\ u(x,0) = u_0, \quad x \in \Omega \end{cases} \tag{1}$$

along with periodic boundary conditions on the rectangular domain $\Omega = \prod_{i=1}^{d}(a_i, b_i) \subset \mathbb{R}^d$. The analysis presented here applies to more general open domains $\Omega \subset \mathbb{R}^d$ with Dirichlet boundary conditions imposed on u and is also applicable with slight modifications for general boundary conditions. Here $u_t = \partial u/\partial t$, $f : \mathbb{R}^d \to \mathbb{R}^d$ is smooth and $\epsilon << 1$ adds a small amount of dissipation. For the analysis in this study this scalar system is useful as model of convection dominated transport and a straightforward example of a nonlinear conservation law system that develops discontinuities and expansions in the context of a Burger's equation model. These mechanisms provide a representative simplified model of the mechanisms that are active in for example an Euler system for ideal fluid flow. With the inclusion of a dissipative operator the effects of diffusion are further introduced as representative of viscous effects that correspond to a Navier-Stokes type system. Hyperbolic PDEs are challenging to solve numerically and often require special treatment for stability. This includes upwinding/Godunov and flux-limiter type methods in the finite-difference/ finite-volume setting, discontinuous Galerkin (DG) finite element methods (FEMs) [1, 2, 3], algebraic flux correction for continuous Galerkin FEM [4, 5, 6], and consistent residual-based stabilized finite element methods with discontinuity capturing type operators for the finite element method [7, 8, 9, 10, 11, 12]. In this study we consider the entropy-viscosity method for the stabilization of numerical approximation of hyperbolic PDEs that is a general method applied to finite difference, spectral methods, and FEM type discretizations and has seen significant recent interest [13, 14, 15]. This method employs an appropriate entropy production residual that corresponds to Equation 1 with $\epsilon = 0$ that can be used to localize the application of numerical dissipation to stabilize the system at discontinuities and sharp internal and boundary-layers with steep under-resolved gradients [13, 14].

In the context of the flexible and accurate time evolution of hyperbolic PDEs with stiff sources or relaxation terms IMEX type schemes have received a significant amount of recent attention [16, 17, 18, 19, 20, 21, 22, 23, 24, 25, 26]. While there are many forms of IMEX discretizations, all IMEX schemes share the basic idea of decomposing the differential operator into two components in which one component is treated implicitly in the discretization and the other component explicitly. This flexibility of mixing explicit and implicit discretization allows the application of specialized numerical solution methods for systems composed of operators with differing time-scales. As an example, consider the case of highly convected flows or shock-physics applications, that also include stiff diffusion and/or nonlinear reaction type mechanisms. In this context a reasonable choice is to employ explicit nonlinear high-resolution methods to the material advection / shock-wave propagation and implicit evaluation for fast

mechanisms (diffusion, reaction) for which optimized implicit solution methods can be designed.

Hyperbolic PDEs are challenging to solve numerically and often have significant discretization errors. The use of complex numerical techniques like IMEX integration and entropy-viscosity further impacts the stability and accuracy of the numerical scheme, and hence it is vital for the reliable use of such schemes in science and engineering that the error be quantified. In this study we employ adjoint based a posteriori analysis to quantify the error in a quantity-of-interest (QoI) using variational analysis and computable residuals of the numerical solution. Adjoint based error estimation is widely used for a host of numerical methods including finite elements, time integration, multi-scale simulations and inverse problems [27, 28, 29, 30, 31, 32, 33, 34, 35, 36, 37, 38, 39]. An appealing feature of the error estimates, that is exploited in this effort, is that the different contributions to the error from various numerical sources can be identified. This characteristic enables the identification of the main source of error/instability in the solution as well as indicating which discretization sources need to be refined to obtain an accurate solution.

The remainder of this paper is organized as follows. Background on IMEX schemes and entropy-viscosity method is described in § 2. This section also outlines the IMEX entropy-viscosity FEM method to solve hyperbolic PDEs. Adjoint based a posteriori analysis is described in § 3. Numerical examples are presented in §4. Finally, conclusions are presented in §5.

2. Numerical Method for Hyperbolic Problems

This section formulates the weak problem corresponding to (1), defines the QoI and presents the IMEX-Entropy-Viscosity method that is employed in this study. We denote the standard space of square integrable functions as $L^2(\Omega)$ with inner product $(\cdot,\cdot)$ and the standard Sobolev space of order 1 as $H^1(\Omega)$.

2.1. Weak form

Let $V \equiv \{v \in H^1(\Omega) | \, v \text{ satisfies periodic boundary conditions}\}$. The continuous weak form corresponding to (1), obtained by multiplying by a test function and integrating second order spatial derivatives by parts, is to find $u \in H^1([0,T]; H^1(\Omega))$ such that

$$\int_0^T (u_t, v) + (\nabla \cdot f(u), v) + (\epsilon \nabla u, \nabla v)\, dt = 0 \tag{2}$$

for all $v \in L^2([0,T]; H^1(\Omega))$. For notational simplicity we define

$$a(\epsilon; u, v) = (\epsilon \nabla u, \nabla v), \qquad b(u, v) = (\nabla \cdot f(u), v). \tag{3}$$

Then (2) is written succinctly as

$$\int_0^T (u_t, v) + b(u, v) + a(\epsilon; u, v)\, dt = 0. \tag{4}$$

2.2. Quantity-of-Interest (QoI)

Often the aim of a numerical simulation is to compute the value of a particular feature of a solution, the so called the quantity-of-interest. Specifically, the quantity-of-interest (QoI) is represented as a a linear functional of the solution to the hyperbolic PDE, and is defined as,

$$Q(u) \equiv (u(x,T), \psi(x)), \tag{5}$$

where $\psi \in L^2(\Omega)$. The QoI (5) considered in this article is based only on the solution at the final time. However, the analysis presented in this article is easily extended to other QoIs like time averaging of the solution. We refer the reader to [40] for the modifications involved.

2.3. Overview of the Entropy-Viscosity method

The problem (1) with $\epsilon = 0$ has a unique entropy solution which satisfies [13, 15]

$$\partial_t E(u) + \nabla \cdot H(u) \leq 0 \tag{6}$$

for any pairs $E(u)$ and $H(u)$ such that E is convex and $H(u) = \int E'(u) f'(u) \mathrm{d}u$. The function E is called entropy and H is the associated entropy flux. We describe the entropy viscosity method for a spatial finite element discretization following the treatment in §2.3 of [13].

We discretize $\Omega \subset \mathbb{R}^d$ into a quasi-uniform triangulation $\mathcal{T}_h$, where h denotes the maximum diameter of the elements. This triangulation is chosen so that the union of the elements of $\mathcal{T}_h$ is Ω and the intersection of any two elements is either a $d-1$ entity (e.g. a common node in one dimension) or is empty. The finite-element approximation is a continuous piecewise polynomial with respect to $\mathcal{T}_h$. We define the standard finite element space consisting of polynomials of degree $\tilde{q}$ as

$$V_h^{(\tilde{q})} = \left\{ v \in C(\Omega) \cap V : \forall K \in \mathcal{T}_h, v|_K \in \mathbb{P}^{\tilde{q}}(K) \right\}. \tag{7}$$

Let $U(\cdot,t) \in V_h \equiv V_h^{(q)}$ be an approximation of the true solution u at time t for a fixed q and entropy pair (E,H). Then the entropy residual D_h is defined as

$$D_h(x,t) = \partial_t E(U) + \nabla \cdot H(U) \tag{8}$$

Further define the viscosity,

$$\nu_E(x,t) = c_E h_K^2 \frac{\|D_h(x,t)\|_{\infty,K}}{\|E(U) - \bar{E}(U)\|_{\infty,\Omega}} \tag{9}$$

where h_K is the diameter of element K containing x, $\bar{E}(U)$ is the average value of the entropy over Ω, and c_E is a scaling that can be set, or held constant over a large class of simulations. An upper bound applied to the numerical viscosity corresponds to upwinding with the maximum propagation speed, defined as

$$\nu_{max}|_K = c_{\max} h_K \| |f'(u)| \|_{\infty,K}. \tag{10}$$

where $f'(u) = \partial f/\partial u$. This leads to the following definition of the entropy-viscosity:

$$\nu_h = \min(\nu_{max}, \nu_E). \tag{11}$$

Note that (9) implies that ν_h is not a constant function. The spatially discretized solution is obtained by the solution of the following semi-discrete equation:

$$(U_t, v) + b(U, v) + a(\epsilon; U, v) + a(\nu_h; U, v) = 0 \tag{12}$$

for all $v \in V_h$.

2.4. An Overview of IMEX Methods

IMEX methods are a time integration technique for a system of ODEs (usually obtained after a method of lines discretization) that treat part of the system explicitly and part implicitly. We describe IMEX methods for a system of ODEs of the form

$$y_t = F(y) + G(y), \qquad t \in (0, T] \tag{13}$$

where $F(y)$ and $G(y)$ refer to the components chosen for explicit and implicit time integration respectively. The extension to PDEs is given later in § 2.5. The time discretization is defined by the nodes

$$0 = t_0 < t_1 < \ldots < t_n < \ldots < t_N = T,$$

with time step $k_n = t_{n+1} - t_n$. For brevity we introduce notation for the subintervals $I_n := [t_n, t_{n+1}]$ and for sub-discretization nodes $t_{n+\tau} := t_n + k_n\tau$ with $\tau \leq 1$.

Multi-stage IMEX schemes are defined by two Butcher tables, one for the explicit method and another for the implicit method,

$$\begin{array}{c|c} \mathbf{c} & A \\ \hline & \mathbf{w} \end{array} \qquad \begin{array}{c|c} \mathbf{d} & B \\ \hline & \tilde{\mathbf{w}} \end{array}, \tag{14}$$

where $A \in \mathbb{R}^{\nu\times\nu}$ and $\mathbf{c}, \mathbf{w} \in \mathbb{R}^{\nu}$ define the explicit method and $B \in \mathbb{R}^{\nu\times\nu}$ and $\mathbf{d}, \tilde{\mathbf{w}} \in \mathbb{R}^{\nu}$ define the implicit method. The components of $A, \mathbf{c}, \mathbf{w}, B, \mathbf{d}$ and $\tilde{\mathbf{w}}$ are denoted as $a_{ij}, c_i, w_i, b_{ij}, d_i$ and $\tilde{w}_i$ respectively for $1 \leq i, j \leq \nu$. Since the A matrix defines an explicit scheme, it must be strictly lower triangular. The implicit schemes we consider are DIRK schemes, therefore the matrix B is lower triangular.

The multi-stage IMEX scheme for (13) is,

$$Y_{n+1} = Y_n + k_n \sum_{i=1}^{\nu} \left[w_i F(\tilde{Y}_i) + \tilde{w}_i G(\tilde{Y}_i) \right], \tag{15}$$

where the stage variables $\tilde{Y}_i$ are given by,

$$\tilde{Y}_i = Y_n + k_n \left[\sum_{j=1}^{i-1} a_{ij} F(\tilde{Y}_j) + \sum_{j=1}^{i} b_{ij} G(\tilde{Y}_j) \right] \tag{16}$$

2.5. The IMEX-Entropy-Viscosity Finite Element Method

The IMEX-Entropy-Viscosity finite element method is obtained by using a multistage IMEX scheme for time integration of (12) on the time interval $[t_n, t_{n+1}]$. The entropy viscosity ν_h is computed from the solutions at previous time steps as in [13]. Then the IMEX Entropy Viscosity Finite Element Method is to find $U_{n+1} \in V_h$ such that,

$$(U_{n+1}, v) = (U_n, v) + k_n \sum_{i=1}^{\nu} \left[w_i F(\tilde{U}_i, v) + \tilde{w}_i G(\tilde{U}_i, v) \right]. \tag{17}$$

Here $F(\tilde{U}_i, v)$ and $G(\tilde{U}_i, v)$ refer to the components chosen for implicit or explicit time integration. Two choices are considered in this paper corresponding to explicit and implicit integration of the entropy-viscosity:

$$F(U, v) = \begin{cases} F_1(U, v) = -b(U, v) - a(\nu_h; U, v), \\ F_2(U, v) = -b(U, v), \end{cases} \tag{18}$$

and

$$G_i(U, v) = -b(U, v) - a(\epsilon; U, v) - a(\nu_h; U, v) - F_i, \qquad i = 1, 2. \tag{19}$$

The stage variables U_i are given by,

$$(\tilde{U}_i, v) = (U_n, v) + k_n \left[\sum_{j=1}^{i-1} a_{ij} F(\tilde{U}_j, v) + \sum_{j=1}^{\nu} b_{ij} G(\tilde{U}_j, v) \right]. \tag{20}$$

3. Adjoint based a posteriori analysis

We employ adjoint based a posteriori analysis to quantify the error in the QoI (5). The error in the QoI given the analytical solution u and a numerical solution obtained from the entropy-viscosity IMEX method U is,

$$Q(u) - Q(U) = Q(u - U) = (u(T) - u_N, \psi) \tag{21}$$

where we used the linearity of the QoI. The a posteriori error estimates are based on variational analysis, adjoint operators and computable residuals.

3.1. Variational Formulation

Adjoint based error estimation relies on variational analysis. An equivalent variational form for the IMEX multi-stage method for a system of ODEs is derived in [40]. This is achieved by defining a nodally equivalent finite element method in time in the sense that the values at time nodes t_n are the same for the FEM and the IMEX scheme. The FEM is in variational form and hence amenable for adjoint based analysis. The extension of the analysis in [40] to the case of PDEs follows directly. We summarize the results below and refer the reader to [40] for details.

3.1.1. The continuous Galerkin FEM in time

On each space-time slab $S_n = \Omega \times I_n$, we choose finite-element approximations that are polynomials of degree q, $\mathbb{P}^q$, in time and continuous piecewise linear polynomials in space with respect to $\mathcal{T}_h$ and define

$$W_n^q = \left\{ w(x,t) : w(x,t) = \sum_{j=0}^{q} t^j v_j(x), \quad v_j \in V_h, \quad (x,t) \in S_n \right\}.$$

The finite element solution is sought in the space W^q where if $v \in W^q$, then $v|_{S_n} \in W_n^q$. The continuous Galerkin method of order $q+1$, cG(q), for (4) is to find $U \in W^q$ such that $U(x,0) = u_0(x)$ and for $n = 0, \ldots, N-1$,

$$\langle (U_t, v) + b(U, v) + a(\epsilon; U, v) \rangle_{I_n} = 0 \quad \forall v \in W_n^{q-1}. \tag{22}$$

where we used the notation

$$\langle \alpha \rangle_{I_n} = \int_{t_n}^{t_{n+1}} \alpha \, dt \tag{23}$$

for functions α defined on I_n.

3.1.2. Equivalent FEM

We define an approximation $\mathcal{I} : H^1([0,T]; H^1(\Omega)) \to L^2([0,T]; H^1(\Omega))$. Denoting the restriction by $\mathcal{I}^n U = \mathcal{I}U|_{I_n}$, the operator is defined by,

$$\mathcal{I}^n U(x,t) = \sum_{i=1}^{\nu} \tilde{U}_i(x) \prod_{j=1, j\neq i}^{\nu} \frac{(t - t_{n+d_j})}{(t_{n+d_i} - t_{n+d_j})}. \tag{24}$$

where $\tilde{U}_i$ are the stage variables for the multi-stage IMEX scheme. We let U_0 be the approximation of u_0 in the discrete space V_h. Using this, the equivalent space-time finite element method is to find $U \in W^q$ such that $U(x,0) = U_0(x)$ and for $n = 0, \ldots, N-1$,

$$\langle (\dot{U}, v_n) \rangle_{I_n} = \langle (F(\mathcal{I}U), v_n) \rangle_{I_n, Q^f} + \langle (G(\mathcal{I}U), v_n) \rangle_{I_n, Q^g} \quad \forall \, v_n \in W_n^{q-1}, \tag{25}$$

where the particular quadratures for the time integration are defined by

$$\langle \varphi \rangle_{I_n, Q^f} = k_n \sum_{i=1}^{\nu} w_i \varphi(t_{n+d_i}), \tag{26}$$

$$\langle \varphi \rangle_{I_n, Q^g} = k_n \sum_{i=1}^{\nu} \tilde{w}_i \varphi(t_{n+d_i}). \tag{27}$$

Note that the operator $\mathcal{I}^n U$ is related to U through (25).

Theorem 1. *The approximation $U(x,t)$ obtained from the space-time finite element method* (25) *is nodally equivalent to the approximation $\{U_n\}$ obtained from the IMEX scheme in* (17) *defined by the Butcher tables* (14).

Proof. The proof is a straightforward extension of Theorem 1 in [40]. □

3.2. Adjoint equations and Error Representations

In this section we develop an adjoint based a posteriori error representation that identifies the total error and decomposes it into contributions from the spatial discretization, implicit and explicit temporal discretizations, and entropy viscosity. Note that there is no unique definition for adjoint operators corresponding to nonlinear operators [41, 42]. We employ a definition based on linearization which is useful for error analysis [29, 27, 43, 44, 36]. The nonlinearity may be present in the function $f(u)$. We define a linearization of this function as

$$\overline{f(u,U)} = \int_0^1 \frac{\partial f}{\partial u}(z)\, \mathrm{d}s, \tag{28}$$

where $z = su + (1-s)U$. Then application of the chain rule and fundamental theorem of calculus implies,

$$f(u) - f(U) = \overline{f(u,U)}(u-U). \tag{29}$$

We define the strong form of the adjoint problem corresponding to (1) as,

$$\begin{cases} -\phi_t(x,t) - \overline{f(u,U)} \cdot \nabla\phi(x,t) = \epsilon\nabla^2\nabla\phi(x,t), \quad t \in [T,0), x \in \Omega \\ \phi(x,T) = \psi, \quad x \in \Omega. \end{cases} \tag{30}$$

Note that the adjoint equation is solved backwards in time from the initial conditions now at T to final time 0. Moreover periodic boundary conditions are imposed ϕ. Note that the imposition of periodic boundary conditions for (1) and (30) are for simplicity. The analysis presented below applies to problems with Dirichlet boundary conditions and requires slight modifications for more general boundary conditions, e.g. see [45].

Lemma 1. *Let $e = u - U$. We have the following error representation for the numerical method in* (22)*,*

$$(e(T),\psi) = (u_0(x) - U_0(x), \phi(x,0)) + \sum_{n=1}^{N-1} \langle -(U_t,\phi) - b(U,\phi) - a(\epsilon;U,\phi)\rangle_{I_n} \tag{31}$$

Proof. Multiplying equation (30) by $(u-U)$ and integrating by parts in space over Ω and in time over I_n leads to

$$-(\phi,e)_{n+1} + (\phi,e)_n + \langle (\phi, u_t - U_t) + (\phi, \nabla\cdot(\overline{f(u,U)}(u-U))) + (\nabla\phi, \epsilon\nabla(u-U))\rangle_{I_n} = 0 \tag{32}$$

where $(\phi,e)_n \equiv (\phi(x,t_n), e(x,t_n))$. Utilizing (29) along with the fact that u is the true solution leads to

$$(\phi,e)_{n+1} = (\phi,e)_n - \langle (\phi,U_t) - (\phi, \nabla\cdot f(U)) - (\nabla\phi, \epsilon\nabla U)\rangle_{I_n} \tag{33}$$

Recursing on $(\phi, e)_n$ and using the initial conditions $u(0) = u_0$, $U(0) = U_0$ and $\phi(T) = \psi$ leads to

$$(u(T)-U_N, \psi) = (u_0-U_0, \phi(x,0))+\sum_{n=1}^{N-1} -\langle(\phi, U_t)-(\phi, \nabla\cdot f(U))-(\nabla\phi, \epsilon\nabla U)\rangle_{I_n} \tag{34}$$

Using the definition of the forms $b(\cdot,\cdot)$ and $a(\cdot;\cdot,\cdot)$ in (3) completes the proof. □

Let $P : V \to V_h$ be a spatial projection operator and $\pi : H^1(I_n) \to \mathcal{P}^{q-1}(I_n)$ be a temporal projection operator. Then the composition $P\pi$ is a projection operator, $P\pi : H^1((I_n); V) \to W_n^{q-1}$ and (25) implies the following Galerkin orthogonality relation,

$$\langle(\dot{U}, P\pi v)\rangle_{I_n} = \langle(F(\mathcal{I}U), P\pi v)\rangle_{I_n,Q^f} + \langle(G(\mathcal{I}U), P\pi v)\rangle_{I_n,Q^g} = 0 \tag{35}$$

for all v in $H_0^1(\Omega) \times H^1(I_n)$.

Theorem 2 (Error Representation)**.** *The error in the quantity-of-interest defined by ψ is given by*

$$(u(T) - U_N, \psi) = E1x + E1t + E2 + E3 + E4 \tag{36}$$

where

$$E1x = E_0+\sum_{n=0}^{N-1} E1x_n, \quad E1t = \sum_{n=0}^{N-1} E1t_n, \quad E2 = \sum_{n=0}^{N-1} E2_n, \quad E3 = \sum_{n=0}^{N-1} E3_n, \quad E4 = \sum_{n=0}^{N-1} E4_n, \tag{37}$$

$$\begin{aligned}
E1x_n &= \langle-(U_t, \phi - P\phi)\rangle_{I_n} + \langle F(\mathcal{I}U, \phi - P\phi)\rangle_{I_n,Q^f} + \langle G(\mathcal{I}U, \phi - P\phi)\rangle_{I_n,Q^g},\\
E1t_n &= \langle-(U_t, P\phi - P\pi\phi)\rangle_{I_n} + \langle F(\mathcal{I}U, P\phi - P\pi\phi)\rangle_{I_n,Q^f} + \langle G(\mathcal{I}U, P\phi - P\pi\phi)\rangle_{I_n,Q^g},\\
E2_n &= \langle F(U, \phi)\rangle_{I_n} - \langle F(\mathcal{I}U, \phi)\rangle_{I_n,Q^f},\\
E3_n &= \langle G(U, \phi)\rangle_{I_n} - \langle G(\mathcal{I}U, \phi)\rangle_{I_n,Q^g},\\
E4_n &= -\langle a(\nu_h; U, \phi)\rangle_{I_n}
\end{aligned} \tag{38}$$

and

$$E_0 = (u_0 - U_0, \phi(0)). \tag{39}$$

Proof. By Lemma 1 and definitions (18), (19) and (39) we have,

$$(e(T), \psi) = E_0 + \sum_{n=1}^{N-1} \langle-(U_t, \phi)\rangle_{I_n} + \langle F(U, \phi) + G(U, \phi) - a(\nu_h; U, \phi)\rangle_{I_n} \tag{40}$$

Adding and subtracting $\langle F(\mathcal{I}U, \phi)\rangle_{I_n,Q^f}$ and $\langle G(\mathcal{I}U, \phi)\rangle_{I_n,Q^g}$ leads to,

$$(e(T), \psi) = E_0+\sum_{n=1}^{N-1} \langle-(U_t, \phi)\rangle_{I_n}+\langle F(U, \phi)\rangle_{I_n,Q^f}+\langle G(U, \phi)\rangle_{I_n,Q^g}+E2_n+E3_n+E4_n \tag{41}$$

Finally, the Galerkin orthogonality relation (35) and adding and subtracting $\langle -(U_t, P\phi)\rangle_{I_n}$, $\langle F(\mathcal{I}U, P\phi)\rangle_{I_n,Q^f}$ and $\langle G(\mathcal{I}U, P\phi)\rangle_{I_n,Q^g}$ completes the proof. □

Remark 1. *The terms $E1x$, $E1t$, $E2$, $E3$ and $E4$ represent the spatial discretization, temporal discretization, explicit, implicit and entropy-viscosity contributions to the error respectively. The term E_0 represents the error due to the approximation of initial conditions in a finite dimensional space. These are signed contributions to the total error and hence there may be significant cancellation between these terms. This is illustrated is the numerical experiments in §4.*

4. Numerical Experiments

Numerical experiments to verify the accuracy of the error estimates and the information about the different contributions of error are conducted for the linear advection-diffusion and damped Burger's equation. Uniform spatial and temporal meshes are used in the experiments. We vary the number of spatial mesh points, N_x, the number of temporal nodes, N_t, turning the entropy-viscosity on or off and different IMEX schemes. The symbol $\Delta t = k_1 = \cdots = k_{N_t}$ refers to the uniform time step size.

The spatial discretization for the forward approximation U is carried out by choosing the space of continuous piecewise linear polynomials, that is, setting $V_h = V_h^{(1)}$. The adjoint solutions are approximated in a higher dimensional FE space. Specifically, the adjoint solutions are solved in the space of continuous piecewise quadratic polynomials, $V_h^{(2)}$ in space and by using the cG(1) method in time but employing time steps 4 times smaller than the steps used in the forward problem. The higher order approximation of the adjoint solution is required for accurate error estimates and is standard in literature [46, 44, 47]. The approximation of the adjoint solution leads to an "error estimate" from the error representation. In theory, the adjoint is obtained by linearizing around a combination of the discrete solution and the true solution. In practice it is common to linearize around the discrete solution only [29] and we follow this approach, that is, we approximate u by U to approximate $f(u, U)$ in (30). This is well established in the literature [27, 29, 48] and produces robust accuracy. Due to the numerical approximation of the adjoint solution and linearization around the discrete solution, the equality in error representation (36) in Theorem 2 no longer holds. Instead, the right-hand side of (36), with the analytical adjoint solution replaced by its numerical approximation gives rise to an error estimate. That is,

$$\text{Estimated Error} = \tilde{E}1x + \tilde{E}1t + \tilde{E}2 + \tilde{E}3 + \tilde{E}4, \tag{42}$$

where the terms $\tilde{E}1x, \tilde{E}1t, \tilde{E}2, \tilde{E}3, \tilde{E}4$ are same as $E1x, E1t, E2, E3, E4$ as defined in (37) and (38) but with the adjoint solution ϕ replaced by its numerical approximation after linearization around the discrete solution. The effectivity

ratio measures the accuracy of the estimate and is defined as,

$$\rho_{\text{eff}} = \frac{\text{Estimated error}}{\text{True error}}.$$

An accurate error estimate has an effectivity ratio close to one.

The IMEX schemes we experiment with are the ARS(2,3,2) and the SSP3(4,3,3) schemes. The names of these schemes are standard and use a triplet notation (s, σ, p) where s is the number of stages in the implicit method, σ is the number of stages in the explicit method, and p is the order of the method as a whole. The Butcher tables for these schemes are shown in Tables 1 and 2.

0	0	0	0
γ	γ	0	0
1	δ	$1-\delta$	0
	0	$1-\gamma$	γ

0	0	0	0
γ	0	γ	0
1	0	$1-\gamma$	γ
	0	$1-\gamma$	γ

Table 1: Butcher Tableau for the explicit(left) and implicit(right) portion of ARS(2,3,2). $\gamma = 1 - \sqrt{2}/2, \delta = -2\sqrt{2}/3$.

0	0	0	0	0
0	0	0	0	0
1	0	1	0	0
1/2	0	1/4	1/4	0
	0	1/6	1/6	2/3

α	α	0	0	0
0	$-\alpha$	α	0	0
1	0	$1-\alpha$	α	0
1/2	β	η	$1/2-\beta-\eta-\alpha$	α
	0	1/6	1/6	2/3

Table 2: Butcher Tableau for the explicit(left) and implicit(right) portion of SSP3(4,3,3). $\alpha = 0.24169426078821, \beta = 0.06042356519705, \eta = 0.12915286960590$

4.1. Linear Advection

The linear advection-diffusion equation is

$$u_t + \nabla \cdot (au) = \epsilon \nabla^2 u, \quad t \in (0, T], x \in \Omega \tag{43}$$

where $\Omega = [0, 1]$, $T = 0.1$, $\epsilon =$ 5E-5 and $a = 1$. The initial conditions are chosen so that $u(x, 0) = 1$ to be one on [0.20, 0.30] and then falling linearly to 0 in an interval of length 0.01. The QoI is represented by choosing ψ to be one on [0.35, 0.45] and then falling linearly to 0 in an interval of length 0.01. In the entropy viscosity method for this scalar equation $E = \frac{1}{2}u^2$ and $H = \frac{1}{2}u^2$ as in [13].

In the results we provide the CFL number and the Péclet number defined respectively as

$$\text{CFL} = \frac{a\Delta t}{h}, \qquad \text{Pe} = \frac{|a|h}{2\epsilon}. \tag{44}$$

Label	Scheme	N_x	N_t	ev	CFL	Pe	$c_{\max}$	F
P1	ARS(2,3,2)	100	20	Off	0.5	500	0.5	F_1
P2	ARS(2,3,2)	200	20	Off	1.0	250	0.5	F_1
P3	ARS(2,3,2)	200	40	Off	0.5	250	0.5	F_1
P4	ARS(2,3,2)	400	30	Off	1.33	125	0.5	F_1
P5	ARS(2,3,2)	400	34	Off	1.176	125	0.5	F_1
P6	SSP3(4,3,3)	400	34	Off	1.176	125	0.5	F_1
P7	SSP3(4,3,3)	400	34	On	1.176	125	0.5	F_1
P8	ARS(2,3,2)	100	20	On	0.5	500	0.5	F_1
P9	ARS(2,3,2)	100	20	On	0.5	500	1.0	F_1
P10	ARS(2,3,2)	100	20	On	0.5	500	1.0	F_2
P11	ARS(2,3,2)	200	40	On	0.5	250	0.5	F_1

Table 3: List of numerical parameters for numerical experiments on (43). Here ev = On corresponds to using the entropy-viscosity method while ev = Off corresponds to setting $\nu_h = 0$. The results are given in Table 4.

Here $h = 1/N_x$ refers to the uniform length of a spatial element. The different sets of parameters and their respective labels chosen for the experiments are shown in Table 3.

The results for parameter P3 and P11 are shown in Figure 1. The difference between the two parameters is that in P3 the entropy-viscosity is turned on while in P11 it is turned off. We observe that the solution without entropy-viscosity has significant over and undershoots while the entropy-viscosity solution is quite stable.

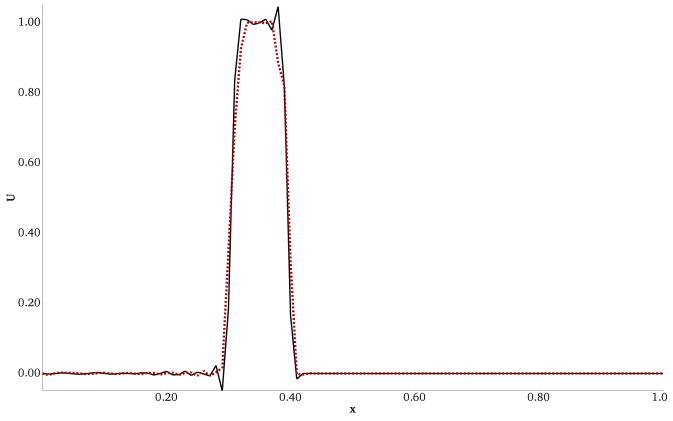

Figure 1: Effect of Entropy-Viscosity for the linear advection equation. Solutions are shown at the final time for P3 (ev = Off) and P11 (ev = On).

The entropy-viscosity is bounded above by the local Lax-Friedrichs (LLF) upwind viscosity. We see this for the linear advection equation for ARS232, $N_x = 100$, $N_t = 20$, $\tau = 0$, $\eta = 0$, $CFL = 0.5, Pe = 500$ in Figure 2. The plots

of the entropy-viscosity is at the initial and final times.

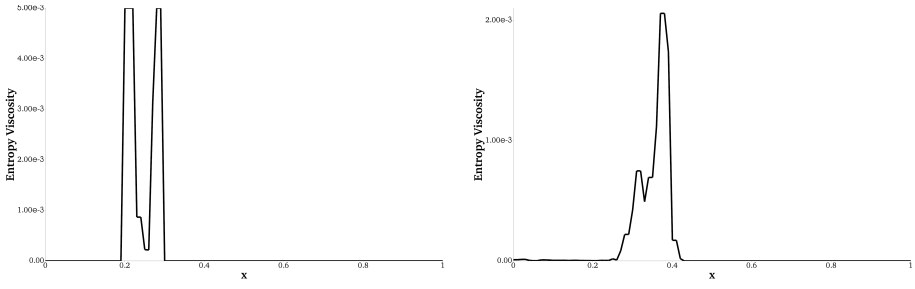

(a) (b)

Figure 2: Plots of Entropy-Viscosity for the linear advection equation for the initial time (left) and final time (right) are shown at the final time for P8. The LLF viscosity is 5E-3.

The results for the errors in the parameters are shown in Table 4.

Label	Err	ρ_{eff}	$\tilde{E}1x$	$\tilde{E}1t$	$\tilde{E}2$	$\tilde{E}3$	$\tilde{E}4$
P1	5.66E-06	1.00	6.46E-05	-2.5E-05	-3.32E-05	-6.9E-07	0
P2	-4.82E-06	1.00	-1.51E-05	3.02E-05	-2.12E-05	1.3E-06	0
P3	-1.07E-05	1.00	-1E-05	-6.46E-07	6.83E-08	-1.05E-07	0
P4	1.04E-02	1.00	-0.005	0.0214	-0.00826	0.00219	0
P5	-3.52E-06	1.00	4.33E-06	1.53E-06	-9.41E-06	3.51E-08	0
P6	-1.63E-06	1.00	1.15E-06	-4.17E-06	1.14E-06	2.43E-07	0
P7	-1.48E-07	1.00	6.92E-07	-2.69E-07	-4.69E-07	3.98E-10	-1.02E-07
P8	-1.51E-05	1.00	1.06E-05	4.97E-06	5.97E-06	-1.68E-07	-3.65E-05
P9	5.36E+12	1.00	6.33E+12	2.49E+12	-3.69E+12	2.23E+11	-5.17E+05
P10	-4.24E-05	1.00	-5.26E-07	-1.39E-06	1.56E-05	4.3E-06	-6.03E-05

Table 4: Results corresponding to the numerical parameters in Table 3. The notation for the parameter settings is provided in Table 3 and the error contributions are defined in (37) and (42).

Initially, in the set of parameters P1–P6 entropy-viscosity is turned off, so the component $\tilde{E}4$ is 0.The error for P1 is dominated by the spatial component $\tilde{E}1x$. The spatial mesh is uniformly refined in P2 and the spatial component $\tilde{E}1x$ shows a marked decrease while the other components of the error remain relatively constant. In P3 we refine the temporal mesh, and as expected the component $\tilde{E}1t$ decreases. However, the total error has actually increased. This is because the component $\tilde{E}2$ for P2 was positive and canceling with the other components which were negative. This component, while having a smaller magnitude, became positive for P3 and hence the cancellation of error was lost and this results in a higher total error, even though the discretization was refined. This scenario is quite common in simulation of complex systems and adjoint based error analysis provides detailed information to determine the cause of

the resulting increase in error even though the temporal component of the discretization has been refined.

In P3 the largest error component is again $\tilde{E}1x$, so in P4 the spatial mesh is refined while the temporal mesh is coarsened. However, the this results in an unstable simulation with a large error. The instability is indicated by the component $\tilde{E}2$ being significant relative to the total error. A stable simulation is obtained by refining in time slightly to get the parameter set P5 since the largest component in P4 is the explicit integration component, $\tilde{E}2$. This can be reduced in two ways: either refining the mesh in time, or by using a higher order method. We investigate the latter next.

In parameter settings P6, the IMEX scheme is switched to SSP3(4,3,3) while the rest of the parameters are the same as in P5. The total error decreases and in particular the component corresponding to explicit integration $\tilde{E}2$ decreases as we expect from a higher order scheme. In P7 the entropy-viscosity is turned on to get an even lower total error, indicating the usefulness of the entropy-viscosity to recover a more accurate representation scheme.

Parameters P8–P10 illustrate features of the IMEX entropy-viscosity method and the error attribution using adjoint based estimates. P8 is similar to P1, but with entropy-viscosity turned on. In P9, the parameter $c_{\max}$ is set to a larger value of 1.0, causing the simulation to be unstable. The component $\tilde{E}2$, indicating the contribution of explicit integration, is larger than $\tilde{E}3$, the component for implicit integration, and this indicates that the instability is caused due to explicit integration of the 2x larger diffusion operator. This is verified in P10, where the entropy-viscosity is now treated in the implicit part and hence leading to a stable simulation.

4.2. Damped Burger's Equation

The damped Burger's equation is

$$u_t + \nabla \cdot (f(u)) = \epsilon \nabla^2 u, \quad t \in (0, T], x \in \Omega \tag{45}$$

here $\Omega = [-1, 1]$, $T = 0.4$, $\epsilon = 5E - 5$ and $f(u) = 0.5u^2$. The initial conditions are represented by the smooth function $u(x, 0) = 100e^{-1/(0.25-x^2)}$ when $|x| < 0.5$ and zero otherwise. The initial conditions are shown in Figure 3. The QoI is represented by choosing ψ to be one on [0.5, 0.6] and then falling to 0 in an interval of length 0.005. This function captures the shock at the final time. In the entropy viscosity method for this scalar equation $E = \frac{1}{2}u^2$ and $H = \frac{1}{3}u^3$ as in [13].

In all simulations for Burger's equation, entropy-viscosity had to be employed to ensure stability. The different parameters are shown in Table 5.

The solution at the final time for P2 and the corresponding entropy-viscosity is shown in Figures 4a and 4b respectively. We observe that the entropy viscosity is an order of magnitude larger than the diffusion parameter ϵ. The solution without the entropy-viscosity is shown in Figure 5 for comparison.

The effectivity ratios are approximated by a highly refined solution with $N_x = 3600$ and $N_t = 3000$. The error and different components for the above parameters ares shown in Table 6.

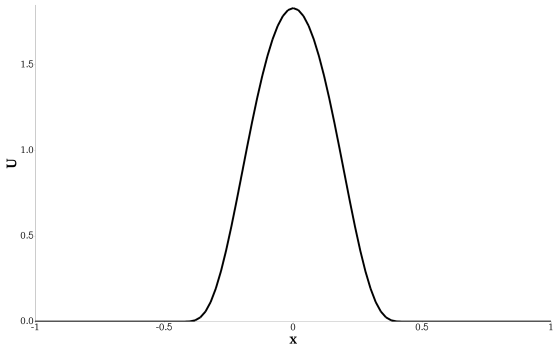

Figure 3: Initial Conditions for Burger's

Label	Scheme	N_x	N_t	$c_{\max}$	F
P1	ARS(2,3,2)	400	333	0.5	F_1
P2	ARS(2,3,2)	600	500	0.5	F_1
P3	ARS(2,3,2)	800	666	0.5	F_1
P4	SSP3(4,3,3)	400	333	0.5	F_1
P5	SSP3(4,3,3)	600	500	0.5	F_1
P6	SSP3(4,3,3)	800	666	0.5	F_1

Table 5: List of numerical parameters for numerical experiments on (45). The results are given in Table 6.

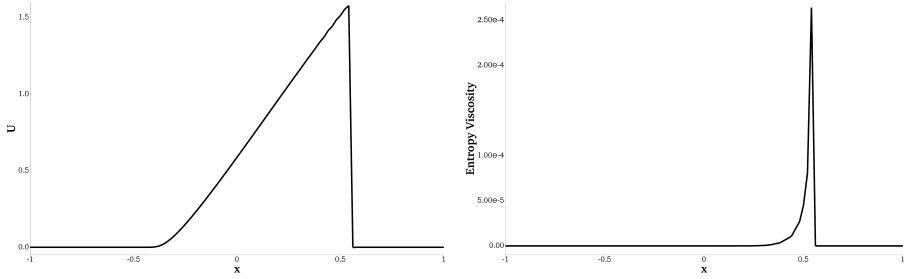

(a) (b)

Figure 4: (a) Burgers Solution at final time for P2 (b) Corresponding entropy viscosity.

.

The effectivity ratios are not as good as those for the linear advection problem. This is expected due to the nonlinear nature of Burgers equation. The ratios approach one as the discretization is refined from P1–P3 and from P4–P6.

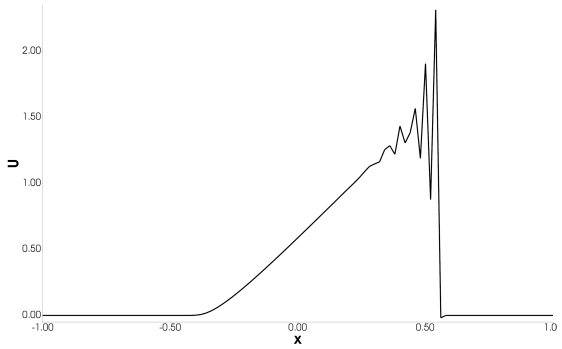

Figure 5: Burgers Solution at final time for results P2 but without using the entropy-viscosity. Compare to Figure 4a.

Label	Err	ρ_{eff}	$\tilde{E}1x$	$\tilde{E}1t$	$\tilde{E}2$	$\tilde{E}3$	$\tilde{E}4$
P1	2.44E-05	0.85	-1.32E-05	1.82E-05	-1.13E-07	-1.35E-08	1.94E-05
P2	6.29E-06	0.88	-5.32E-06	5.77E-06	-3.97E-08	-2.47E-09	5.89E-06
P3	3.15E-06	0.97	-5.37E-07	1.86E-06	-3.22E-08	-7.31E-10	1.86E-06
P4	2.43E-05	0.85	-1.32E-05	1.83E-05	-6.9E-08	-2.78E-09	1.93E-05
P5	6.32E-06	0.88	-5.26E-06	5.75E-06	1.17E-08	-7.28E-10	5.83E-06
P6	3.18E-06	0.98	-4.95E-07	1.83E-06	3.03E-09	-1.08E-10	1.83E-06

Table 6: Results corresponding to the numerical parameters in Table 5. The notation for the error contributions is defined in (37).

4.3. The case of vanishing diffusion

We conduct a series of experiments showing the stability of the error estimates as ϵ decreases to 0. The results for the parameter P2 in Table 3 for linear advection are shown in Table 7. The results for Burgers corresponding to parameter P2 in Table 5 are shown in Table 8.

ϵ	Err	ρ_{eff}	$\tilde{E}1x$	$\tilde{E}1t$	$\tilde{E}2$	$\tilde{E}3$	$\tilde{E}4$
5E-05	-4.82E-06	1.00	-1.51E-05	3.03E-05	-2.13E-05	1.29E-06	0
1E-06	$3.82E-06$	0.98	5.2E-06	-2.79E-07	-1.79E-06	1.31E-10	6.93E-07
1E-07	$3.83E-06$	0.98	5.1E-06	-2.71E-07	-2.02E-06	-1.39E-12	1.02E-06

Table 7: Results corresponding to P2 in Table 3 as ϵ goes to 0 for linear advection equation, see (43).

The entropy-viscosity at the final time for ϵ = 1E-7 is shown in Figure 6. The entropy-viscosity is now three orders of magnitude (3E-4 vs. 1E-7) larger compared to ϵ. As ϵ goes to zero, the solution develops a sharp layer which is not accurately resolved by the spatial mesh and hence linearization of the adjoint solution around the discrete solution causes the accuracy of the adjoint

ϵ	Err	ρ_{eff}	$\tilde{E}1x$	$\tilde{E}1t$	$\tilde{E}2$	$\tilde{E}3$	$\tilde{E}4$
5E-05	6.29E-06	0.88	-5.32E-06	5.77E-06	-3.97E-08	-2.47E-09	5.89E-06
1E-06	$1.47E-05$	1.46	-2.31E-05	1.91E-05	1.21E-06	9.84E-10	1.75E-05
1E-07	$1.77E-05$	1.76	-2.87E-05	2.16E-05	5.33E-06	6.6E-10	1.95E-05

Table 8: Results corresponding to P2 in Table 5 as ϵ goes to 0 for Burgers equation, see (45).

solution to degrade [47]. Thus we see that the effectivity ratio for ϵ = 1E-07 is not as accurate as that for smaller values of ϵ, a phenomenon also observed in [47].

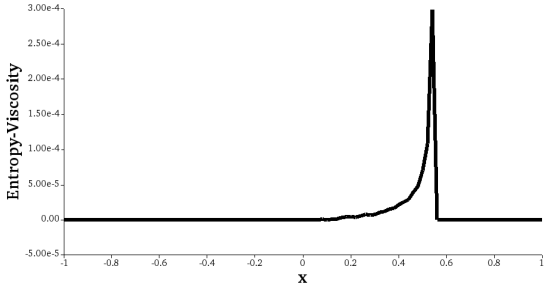

Figure 6: Entropy-viscosity for ϵ = 1E-7.

4.4. 2D Linear Advection

Consider (43) in two dimensions with $a = [1, 0]^T$, $\Omega = [0, 1]$, $T = 0.1$, ϵ = 5E-5 with non-smooth initial conditions set as $u(\mathbf{x}, 0) = 1$ on $[0.2, 0.3]\times[0.2, 0.3]$ and falling linearly to 0 on the adjacent grid point. The QoI is defined by choosing $\psi(x) = \sin(2\pi x)\sin(2\pi y)$. Moreover, we set ϵ = 1E-6.

The parameters for the experiment are shown in Table 9. The errors in these parameters is shown in Table 10. In the first three parameters, P1–P3, 20 timesteps are used. Notice that the error increases when we turn on the entropy-viscosity in going from P1 to P2. However, an examination of the components of error indicate the reason: the largest component of the error is $\tilde{E}2$, that is, the contribution due to explicit integration. Integrating the entropy-viscosity explicitly causes an instability in the simulation. This is also seen in Figure 7 showing the solution at the final time for parameters P2 and P3. Making the entropy-viscosity implicit in P3 results in a significant reduction in error as witnessed in P3. The error in P3 is also significantly less than P1, that is, entropy-viscosity again results in a desirable decrease in total error provided it is integrated appropriately. Parameters P4–P6 are performed with 40 timesteps. Turning on the entropy-viscosity in P5 and P6 results in a significant decrease in the error when contrasted with P4 where the entropy-viscosity was turned off. Moreover, both implicit and explicit integration of the entropy-viscosity are stable in this case.

Label	Scheme	N_x	N_t	ev	$c_{\max}$	F
P1	ARS(2,3,2)	100	20	Off	0.5	F_1
P2	ARS(2,3,2)	100	20	On	0.5	F_1
P3	ARS(2,3,2)	100	20	On	0.5	F_2
P4	ARS(2,3,2)	100	40	Off	0.5	F_1
P5	ARS(2,3,2)	100	40	On	0.5	F_1
P6	ARS(2,3,2)	100	40	On	0.5	F_2

Table 9: List of numerical parameters for numerical experiments on (43). The results are given in Table10.

Label	Err	ρ_{eff}	$\tilde{E}1x$	$\tilde{E}1t$	$\tilde{E}2$	$\tilde{E}3$	$\tilde{E}4$
P1	-1.18E-05	1.00	-1.84E-05	2.1E-06	4.45E-06	-6.56E-11	0
P2	-3.57E-04	1.00	-0.000675	-0.00054	0.000701	-1.35E-07	0.000156
P3	1.33E-07	1.23	-7.14E-07	3.04E-07	5.43E-07	-2.7E-06	2.7E-06
P4	-1.45E-05	1.00	-1.55E-05	3.53E-07	6.69E-07	-1.13E-10	0
P5	-5.71E-07	0.95	-6.41E-06	9.16E-07	9.62E-08	-2E-11	4.82E-06
P6	-5.69E-07	0.95	-1.61E-06	9.88E-07	5.13E-08	-4.69E-06	4.69E-06

Table 10: Results corresponding to the numerical parameters in Table 9. The notation for the error contributions is defined in (37).

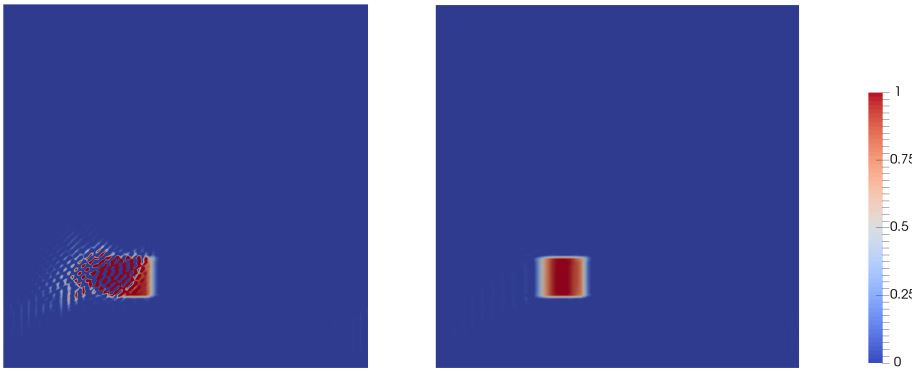

(a) (b) (c)

Figure 7: Plots of the solution at the final time for parameters P2 (left) and P3 (right) in table 9. Explicit integration of the entropy-viscosity leads to unstable oscillations in the solution while implicit integration is stable.

5. Conclusions

This study considered adjoint based a posteriori error estimates for numerical solutions of an implicit-explicit (IMEX) time integration of an entropy-viscosity formulation for scalar hyperbolic conservation law equations. The numerical

examples were comprised of linear advection and Burgers equation with the introduction of a small amount of dissipation. The adjoint analysis was demonstrated to provide error estimates for both the spatial and temporal approximations, with component estimates for the IMEX partition of the system into explicit and implicit operators. The numerical results confirmed the adjoint analysis and provided a demonstration that the analysis provides reasonable estimates and identification of the contribution of the various sources of the errors to the total error. In this context examples were presented that identified the largest components and either refined the spatial or temporal approximation, or switched the assignment of operators from explicit to implicit IMEX treatment to reduce the total error. Further work will consider possibly alternate definitions of entropy viscosity for these systems and also extend the analysis to the Euler equations for which the Burgers system is just a partial model of expansions and shocks.

Acknowledgments

Jehanzeb H. Chaudhry's work is supported in part by the National Science Foundation (DMS-1720402) and Sandia National Laboratories: Laboratory Directed Research and Development (LDRD) Funding under Academic Alliance Program FY2016.

References

[1] B. Cockburn, C.-W. Shu, The Runge–Kutta discontinuous Galerkin method for conservation laws V: multidimensional systems, Journal of Computational Physics 141 (2) (1998) 199–224.

[2] B. Cockburn, C.-W. Shu, Runge–Kutta discontinuous Galerkin methods for convection-dominated problems, Journal of scientific computing 16 (3) (2001) 173–261.

[3] J. S. Hesthaven, T. Warburton, Nodal discontinuous Galerkin methods: algorithms, analysis, and applications, Springer Science & Business Media, 2007.

[4] D. Kuzmin, On the design of general-purpose flux limiters for finite element schemes. I. Scalar convection, Journal of Computational Physics 219 (2) (2006) 513–531.

[5] D. Kuzmin, M. Möller, Algebraic flux correction I. Scalar conservation laws, in: Flux-corrected transport, Springer, 2005, pp. 155–206.

[6] D. Kuzmin, S. Turek, High-resolution FEM-TVD schemes based on a fully multidimensional flux limiter, Journal of Computational Physics 198 (1) (2004) 131–158.

[7] T. J. R. Hughes, Recent progress in the development and understanding of SUPG methods with special reference to the compressible Euler and Navier-Stokes equations, Int. J. Numer. Meth. Fluids 7 (11) (1987) 1261–1275.

[8] T. J. R. Hughes, L. P. Franca, G. M. Hulbert, A new finite element formulation for computational fluid dynamics: VIII. The Galerkin/least-squares method for advective-diffusive equations, Computer Methods in Applied Mechanics and Engineering 73 (2) (1989) 173 – 189.

[9] T. J. Hughes, G. Scovazzi, T. E. Tezduyar, Stabilized methods for compressible flows, Journal of Scientific Computing 43 (3) (2010) 343–368.

[10] V. John, P. Knobloch, On spurious oscillations at layers diminishing (SOLD) methods for convection–diffusion equations: Part I–A review, Computer Methods in Applied Mechanics and Engineering 196 (17) (2007) 2197–2215.

[11] R. Codina, A discontinuity-capturing crosswind-dissipation for the finite element solution of the convection-diffusion equation, Computer Methods in Applied Mechanics and Engineering 110 (3-4) (1993) 325–342.

[12] F. Shakib, Finite element analysis of the compressible Euler and Navier-Stokes equations, Ph.D. thesis, Stanford University (1989).

[13] J.-L. Guermond, R. Pasquetti, B. Popov, Entropy viscosity method for nonlinear conservation laws, Journal of Computational Physics 230 (11) (2011) 4248–4267.

[14] J.-L. Guermond, B. Popov, V. Tomov, Entropy-viscosity method for the single material Euler equations in Lagrangian frame, Computer Methods in Applied Mechanics and Engineering 300 (2016) 402 – 426.

[15] J.-L. Guermond, M. Nazarov, B. Popov, Y. Yang, A second-order maximum principle preserving lagrange finite element technique for nonlinear scalar conservation equations, SIAM J. Numer. Anal. 52 (2014) 2163–2182.

[16] L. Pareschi, G. Russo, Implicit-Explicit Runge-Kutta schemes and applications to hyperbolic systems with relaxation, Journal of Scientific Computing. 25 (112) (2005) 129–154.

[17] W. Hundsdorfer, S. J. Ruuth, IMEX extensions of linear multistep methods with general monotonicity and boundedness properties, J. Comput. Phys. 225 (2) (2007) 2016–2042.

[18] R. Donat, I. Higueras, A. Martinez-Gavara, On stability issues for IMEX schemes applied to 1D scalar hyperbolic equations with stiff reaction terms, Math. Comp. 276 (2011) 2097–2126.

[19] M. Svard, S. Mishra, Implicit-explicit schemes for flow equations with stiff source terms, J. Comp. and Applied Math. 235 (2011) 1564–1577.

[20] U. M. Ascher, S. J. Ruuth, B. T. R. Wetton, Implicit-explicit methods for time-dependent partial differential equations, SIAM Journal on Numerical Analysis 32 (3) (1995) pp. 797–823.

[21] U. M. Ascher, S. J. Ruuth, R. J. Spiteri, Implicit-explicit Runge-Kutta methods for time-dependent partial differential equations, Appl. Numer. Math. 25 (2-3) (1997) 151–167.

[22] M. H. Carpenter, C. A. Kennedy, H. Bijl, S. A. Viken, V. N. Vatsa, Fourth-order Runge-Kutta schemes for fluid mechanics applications, Journal of Scientific Computing 25 (112) (2005) 157–194.

[23] E. M. Constantinescu, A. Sandu, Extrapolated implicit-explicit time stepping, SIAM Journal on Scientific Computing 31 (6) (2010) 4452–4477.

[24] A. Cardone, Z. Jackiewicz, A. Sandu, H. Zhang, Extrapolated implicit-explicit Runge-Kutta methods, Mathematical Modelling and Analysis 19 (1) (2014) 18–43.

[25] E. Zharovsky, A. Sandu, H. Zhang, A class of implicit-explicit two-step Runge–Kutta methods, SIAM J. Numer. Anal. 53 (1) (2015) 321–341.

[26] H. Zhang, A. Sandu, S. Blaise, Partitioned and implicit-explicit general linear methods for ordinary differential equations, Journal of Scientific Computing 61 (1) (2014) 119–144.

[27] D. Estep, *A posteriori* error bounds and global error control for approximation of ordinary differential equations, SIAM J. Numer. Anal. 32 (1) (1995) 1–48.

[28] K. Eriksson, D. Estep, P. Hansbo, C. Johnson, Computational Differential Equations, Cambridge University Press, Cambridge, 1996.

[29] D. Estep, M. Larson, R. Williams, Estimating the error of numerical solutions of systems of reaction-diffusion equations, Memoirs of the American Mathematical Society 146 (696).

[30] M. Ainsworth, T. Oden, *A posteriori* error estimation in finite element analysis, John Wiley-Teubner, 2000.

[31] W. Bangerth, R. Rannacher, Adaptive Finite Element Methods for Differential Equations, Birkhauser Verlag, 2003.

[32] T. J. Barth, *A posteriori* Error Estimation and Mesh Adaptivity for Finite Volume and Finite Element Methods, Vol. 41 of Lecture Notes in Computational Science and Engineering, Springer, New York, 2004.

[33] R. Becker, R. Rannacher, An optimal control approach to *a posteriori* error estimation in finite element methods, Acta Numerica (2001) 1–102.

[34] M. B. Giles, E. Süli, Adjoint methods for PDEs: a posteriori error analysis and postprocessing by duality, Acta Numerica 11 (1) (2002) 145–236.

[35] Y. Cao, L. Petzold, A posteriori error estimation and global error control for ordinary differential equations by the adjoint method, SIAM Journal on Scientific Computing 26 (2) (2004) 359–374.

[36] J. H. Chaudhry, D. Estep, V. Ginting, J. N. Shadid, S. Tavener, A posteriori error analysis of IMEX multi-step time integration methods for advection–diffusion–reaction equations, Computer Methods in Applied Mechanics and Engineering 285 (2015) 730–751.

[37] J. B. Collins, D. Estep, S. Tavener, A posteriori error analysis for finite element methods with projection operators as applied to explicit time integration techniques, BIT Numerical Mathematics 55 (4) (2015) 1017–1042.

[38] V. Rao, A. Sandu, A posteriori error estimates for the solution of variational inverse problems, SIAM/ASA Journal on Uncertainty Quantification 3 (1) (2015) 737–761.

[39] J. Jakeman, T. Wildey, Enhancing adaptive sparse grid approximations and improving refinement strategies using adjoint-based a posteriori error estimates, Journal of Computational Physics 280 (2015) 54–71.

[40] J. H. Chaudhry, J. Collins, J. N. Shadid, A posteriori error estimation for multi-stage Runge-Kutta IMEX schemes, Applied Numerical Mathematics 117 (2017) 36–49.

[41] G. I. Marchuk, V. I. Agoshkov, V. P. Shutyaev, Adjoint equations and perturbation algorithms in nonlinear problems, CRC Press, 1996.

[42] G. I. Marchuk, Adjoint Equations and Analysis of Complex Systems, Springer Nature, 1995.

[43] K. Eriksson, D. Estep, P. Hansbo, C. Johnson, Introduction to adaptive methods for differential equations, in: Acta Numerica, 1995, Acta Numerica, Cambridge Univ. Press, Cambridge, 1995, pp. 105–158.

[44] J. H. Chaudhry, D. Estep, S. Tavener, V. Carey, J. Sandelin, A posteriori error analysis of two-stage computation methods with application to efficient discretization and the Parareal algorithm, SIAM Journal on Numerical Analysis 54 (5) (2016) 2974–3002.

[45] W. T., T. S., E. D., A posteriori error estimation of approximate boundary fluxes, Communications in Numerical Methods in Engineering 24 (6) (2008) 421–434.

[46] B. Aksoylu, S. D. Bond, E. C. Cyr, M. Holst, Goal-oriented adaptivity and multilevel preconditioning for the Poisson-Boltzmann equation, Journal of Scientific Computing 52 (1) (2011) 202–225.

[47] J. B. Collins, D. Estep, S. Tavener, A posteriori error estimation for the Lax–Wendroff finite difference scheme, Journal of Computational and Applied Mathematics 263 (2014) 299–311.

[48] D. Estep, Error estimates for multiscale operator decomposition for multiphysics models, in: J. Fish (Ed.), Multiscale methods: bridging the scales in science and engineering, Oxford University Press, USA, 2009.

[49] M. Giles, S. Ulbrich, Convergence of linearized and adjoint approximations for discontinuous solutions of conservation laws. part 2: Adjoint approximations and extensions, SIAM J. Numer. Anal. 48 (3) (2010) 905–921.